Rock and Soil Mechanics

Volume 43 | Issue 3 Article 5

5-17-2022

Research on the failure precursors of layered slate based on multifractal characteristics of acoustic emission

Bo SUN
School of Mining Engineering, University of Science and Technology Liaoning, Anshan, Liaoning 114000, China

Fu-qiang REN
State Key Laboratory for GeoMechanics and Deep Underground Engineering, China University of Mining and Technology, Beijing 100083, China, renfuqiangcumtb@163.com

Dong-qiao LIU
State Key Laboratory for GeoMechanics and Deep Underground Engineering, China University of Mining and Technology, Beijing 100083, China

Custom Citation

SUN Bo, REN Fu-qiang, LIU Dong-qiao, . Research on the failure precursors of layered slate based on multifractal characteristics of acoustic emission[J]. Rock and Soil Mechanics, 2022, 43(3): 749-760.

Rock and Soil Mechanics 2022 43(3): 749−760 ISSN 1000−7598
https: //doi.org/10.16285/j.rsm.2021.5879 rocksoilmech.researchcommons.org/journal

Research on the failure precursors of layered slate based on multifractal characteristics of acoustic emission

SUN Bo[1], REN Fu-qiang[2, 3], LIU Dong-qiao[3]

1. School of Mining Engineering, University of Science and Technology Liaoning, Anshan, Liaoning 114000, China
2. School of Civil Engineering, University of Science and Technology Liaoning, Anshan, Liaoning 114000, China
3. State Key Laboratory for GeoMechanics and Deep Underground Engineering, China University of Mining and Technology, Beijing 100083, China

Abstract: In order to explore the failure precursors of layered slate, five groups of slate with different bedding angles (β= 0°, 30°, 45°, 60° and 90°) were carried out using uniaxial compression tests, and the failure mode, acoustic emission (AE) parameters and multifractal characteristics are analyzed. The relationship between multifractal spectrum width ($\Delta\alpha$) and damage evolution was discussed, and the precursor and warning time of final failure based on multifractal were determined. The results indicate that: when the bedding angle β increases from 0° to 90°, the failure modes of slate firstly change from tension-splitting failure to splitting-shear, then to shear slip, and finally to tension-splitting. The sudden increase of AE counts and the continuous increase in low-frequency (LF) and high-amplitude (HA) signals can be identified as precursors for predicting the failure of rocks. The proportions of LF-HA signals in the crack coalescence stage firstly decrease and then increase with the increase of bedding angle, β. Furthermore, the time of the sudden increase in $\Delta\alpha$ occurs before the damage mutation, in details, with the increase of β, the early warning time of $\Delta\alpha$ increases first, then decreases and then increases again, and the early warning time of slate (β= 30°) is the longest.

Keywords: slate; bedding angle; acoustic emission; multifractal; failure precursor

1 Introduction

As a metamorphic rock with significant bedding structures in many layered rock masses in underground engineering such as roadway and tunnel, slate is susceptible to different forms of failure and controls the stability of underground structure[1]. Therefore, it is of great significance to understand the failure mechanism and precursors of layered slate for underground engineering construction and stability control. Numerous studies have been conducted on the failure mechanism and mechanical properties for different layered rocks. For example, Liu et al.[2] found that coal with different layered dip angles presents obvious anisotropy characteristic. Ye et al.[3] carried out Brazilian splitting test of slate and analyzed its microscopic failure mechanism. Tavallali et al.[4] emphasized the influence of microscopic parameters of layered sandstone on macroscopic characteristics. Ning et al.[5] studied the successive failure process of layered slate through particle flow numerical analysis and discussed its failure mechanism. Ou et al.[6] discussed the mechanical properties and fracture mechanism of layered slate by using split Hopkinson pressure bar. Wu et al.[7] found that the strength of layered phyllite increases first and then decreases with the increase of dip angle by using the split Hopkinson impact tests. Li et al.[8], Sun et al.[9] and Chu et al.[10] found that the variation of slate compressive strength presents an "U" shape with the increase of bedding dip angle β. Wang et al.[11] systematically analyzed the mechanical properties of shale with different bedding angles, and concluded that with the increase of bedding angle, the elastic modulus of shale encounters the "decrease and the following increase" twice.

In practical engineering, the precursors of rock instability are the premise of disaster warning of rockburst[12]. At present, numerous results have been achieved to analyze the precursors of rock fracture by using the evolution characteristics of acoustic emission (AE) signal. Ganne et al.[13] studied the correlation between microcracks and AE. Diao et al.[14] analyzed the variation of AE ringing count of slate with multiple bedding angles and pointed out that the sudden increase of ringing count could be used as a precursor of slate instability. Through uniaxial compression test, Li et al.[15] suggested that AE quiet period, energy rate, ringing count rate and volume expansion

Received: 11 June 2021 Revised: 15 December 2021
This work was supported by the National Natural Science Foundation of China(52074299), the State Key Laboratory for GeoMechanics and Deep Underground Engineering, China University of Mining & Technology, Beijing (SKLGDUEK2128) and the Excellent Young Scientific and Technological Talents Project of University of Science and Technology, Liaoning(2021YQ02).
First author: SUN Bo, male, born in 1995, Postgraduate, focused on rock mechanics. E-mail: 1542281232@qq.com
Corresponding author: REN Fu-qiang, male, born in 1992, PhD, Lecturer, research interests: rock mechanics and rockburst control. E-mail: renfuqiangcumtb@163.com

can be used as precursor indicators of rock instability failure. Through AE frequency domain characteristics monitoring, Wang et al.[16] proposed that the increase in the proportion of low-frequency (LF) high-amplitude (HA) signals could be used as precursor of rock instability. Li et al.[17] carried out the research on rock instability precursor identification based on the spatial-temporal evolution of AE. Fractal theory has also been widely applied in the analysis of AE signals in rock failure process. For example, Yin et al[18], Cong et al.[19], Xu et al.[20] proposed that the continuous decline of fractal dimension could be regarded as precursors of rock failure. Yuan et al.[21] analyzed the relationship between fractal dimension and rock strength during rock failure. Xu et al.[22] studied the similarity of fractal characteristics of rock AE signals. Kong et al.[23] calculated the fractal dimension of time series of coal samples and found that the fractal dimension develops from chaos to orderly state, making it an explicit failure precursor of coal.

Because of the nonlinear and inhomogeneous rock failure process, simple fractals cannot reflect its macroscopic mechanism. Therefore, the analysis of AE multifractal characteristics enables us to understand the law of rock fracture. Cai et al.[24] deconstructed the characteristics of AE signals via multifractal and expounded the complexity of rock failure. Yang et al.[25] adopted the box counting method to calculate the multifractal spectrum of heterogeneous rock before the uniaxial loading reaches the peak value, and found that as the load increases, the effect of large probability subset is obvious. Zhang et al.[26] proposed that the dynamic changes of multifractal spectrum parameters $\Delta\alpha$ and $\Delta f(\alpha)$ reflect the stress and failure states of coal samples by analyzing the multifractal characteristics of AE signals. Kong et al.[27] stated that multifractal parameters could accurately represent the damage evolution of coal. Xu et al.[28] analyzed the variation of multifractal parameters $\Delta\alpha$and $\Delta f(\alpha)$ at each failure stage, and suggested that their variation trends at different stages can be used as precursors of rock instability warning.

Overall, most of the studies on the layered rock focus on the mechanical properties and fracture mechanism. However, the research on the influence of bedding dip angle on the precursor of rock instability, especially multifractal precursors, is overlooked. In this study, uniaxial compression tests of slates with different bedding dip angles (0º, 30º, 45º, 60º and 90º) are carried out to explore the failure precursors of layered slates in combination with macro failure characteristics, AE parameters and multifractal characteristics, aiming to provide theoretical basis for the stability evaluation and monitoring of layered rock.

2 Experiments

2.1 Rock samples

The layered slate samples were taken from the #2 inclined well of the extra long tunnel in Muzhailing, Gansu Province. The samples were cored into standard cylinders with bedding dip angle of 0º, 30º, 45º, 60º and 90º, respectively. Each group contains 3 specimens with average density of 2.68 g/cm^3. The X-ray diffraction analysis manifests that the slate is mainly composed of quartz (50.3%) and clay minerals (46.9%). The microstructure is shown in Fig.1(b). The main components of clastic clay minerals are quartz, feldspar and mica, with

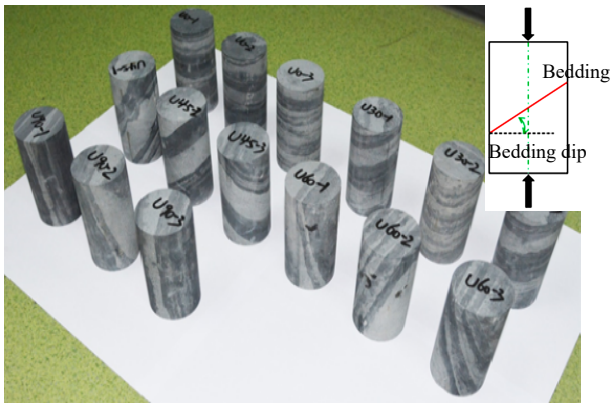

(a) The sample of layered slate

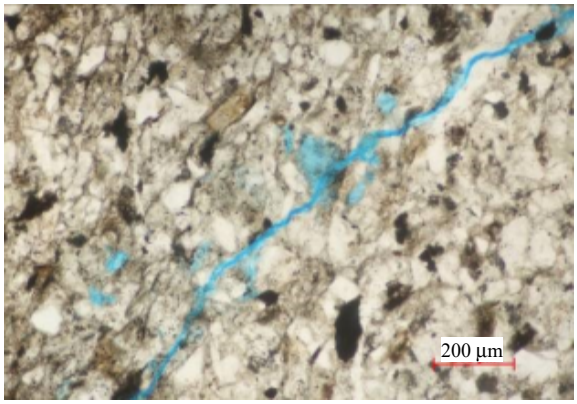

(b) The microstructures within in slate

Fig. 1 The photograph and microstructure of slate

a small amount of calcite. The clastic clay minerals are mainly illite, accounting for 47%, followed by chlorite (25%). The micropores of the samples range from 0.01 mm to 0.12 mm, and are mainly point-to-line contact. Microcracks are 0.01 mm in width in average and are distributed locally.

2.2 Experimental setup

The uniaxial compression test was carried out using a 2 000 kN hydraulic servo single triaxial test system (as shown in Fig.2). The upper and lower pads (20 mm from the end) of the samples were mounted with AE sensors, respectively. Coupling agent was applied between the samples and the sensors to ensure close contact. The Nano-30 sensor from Acoustic Physics Company of America was used in this study. The frequency response range of the tensors is 100−400 kHz, and the sampling rate of AE signal is set as 2 MHz. A preload of 2 kN was applied before the test, and then the sample was loaded at a loading rate of 0.01 mm/min until failure.

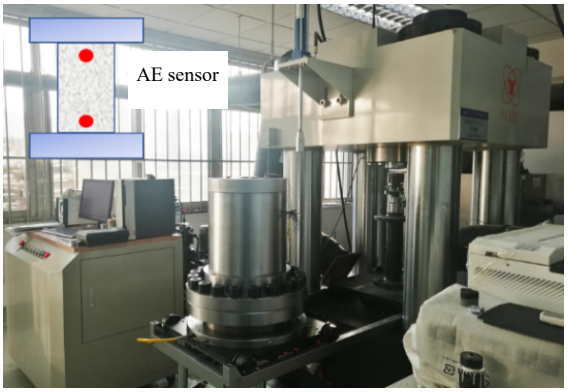

Fig. 2 Experimental equipment

3 Results

3.1 Failure characteristics of layered slate

Figure 3 shows the stress-strain curves of slates with different bedding dip angles. The peak strength first

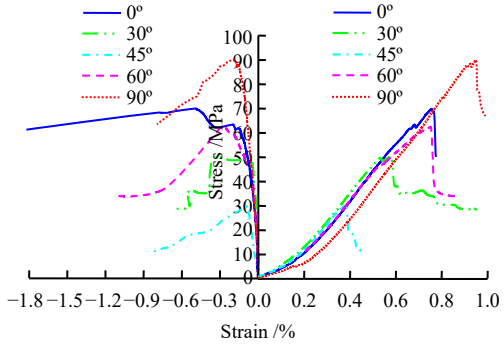

Fig. 3 Stress−strain curves of layered slate

increases and then decreases with the increase of bedding dip angle. The maximum and minimum peak stresses are 89.93 MPa and 29.69 MPa, respectively, corresponding to 0° and 45° dip angles. The axial strain corresponding to peak stress varies significantly and presents obvious anisotropy.

Figure 4 depicts the failure types of five groups of slates. When the bedding dip angle β is 0°, the sample exhibits tensile splitting failure cross the bedding planes. Due to the Poisson effect, horizontal tensile stress is produced under the action of axial stress, and several vertical cracks cutting through the bedding appear. The failure mode of slate with 30° dip angle are splitting and shear failure through and along the bedding. The shear cracks along the bedding plane occur in somewhere, and the rest cracks cut through the bedding and develop in multi-segmentary folds.

When the dip angle increases to 45° and 60°, the slate exhibits shear slip failure along the bedding plane. The occurrence of slip cracks indicate that the maximum shear stress of the bedding plane exceeds the shear strength, that is, the failure of slates with bedding dip angles of 45° and 60° is controlled by the bedding plane. The failure mode of slate with 90° dip angle is tension-splitting failure along the bedding. Under uniaxial load, tensile cracks occur along the bedding. As the sample can still bear load after fracturing, the sample is bent and split afterwards during the process of continued loading, and microcracks are connected to form macrocracks.

To sum up, as the dip angle increases from 0° to 90°, the failure modes of slate under uniaxial load change from tension-splitting failure through bedding to splitting and shear fracturing through and locally along bedding, then to shear slip along bedding, and finally to tension-splitting along bedding. This conclusion is basically consistent with the phenomenon described in References [29−30], indicating that the experimental results in this study are reliable.

3.2 Characteristics of AE parameters

3.2.1 AE activity

Figure 5 shows the relationship between AE ringing count, cumulative ringing count and stress−time in the loading of layered slate. The deformation process can be divided into five stages[31−32]: (a) Compaction stage (*ab*); (b) Elastic stage (*bc*); (c) Initial cracking stage (*cd*); (d)

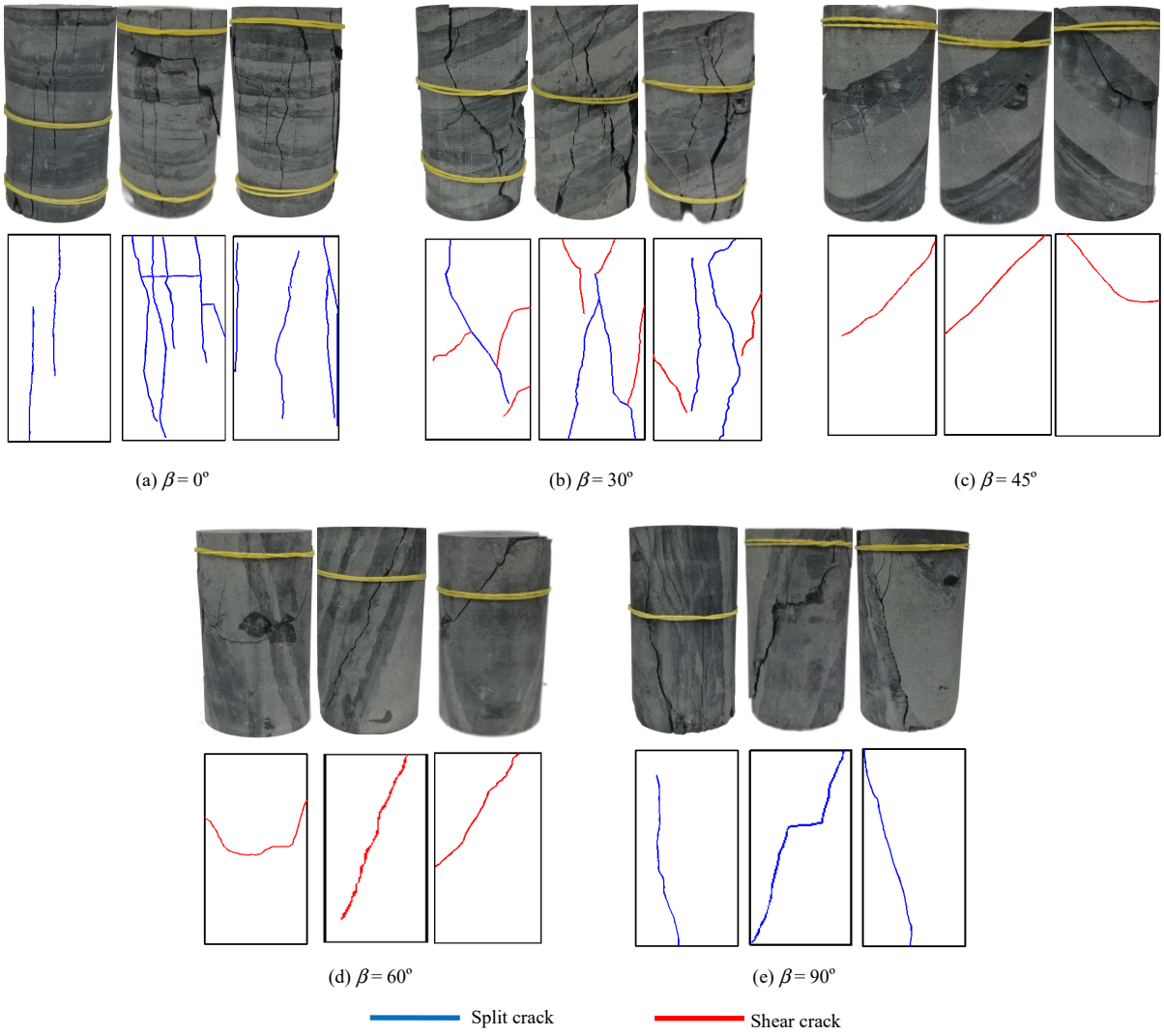

Fig. 4 Typical failure patterns of layered slate

Crack transfixion stage (*de*); (e) Post-peak stage (*ef*), where *c*, *d* and *e* correspond to the damage stress σ_{cd}, crack initiation stress σ_{ci} and peak stress σ_c, respectively.

In Fig.5, with the continuous increase of stress, the changes of AE ring count in different stages are distinct. In stage *ab*, cracks in the slate are gradually compacted, resulting in a small quantity of microcracks. The AE ring counts of 0°, 30°, 45° and 60° dip angle samples are low, and the cumulative ring counts have likely hit a plateau. The axial stress of slate with 90° dip angle follows the bedding plane, resulting in locally developed cracks, dense AE signals, and a significant increase in cumulative ringing count. When entering the stage *bc*, the internal microcracks are compacted continuously, without new cracks formed in slate. The change of cumulative ringing count is unobvious. As the stress increases to stage *cd*, the microcracks in the slates with 0°, 45° and 60° dip angles gradually develop. The AE ring count increases gradually, and the cumulative ring count curve steepens accordingly. While the 30° and 90° dip angle samples produce less AE signals. Meanwhile, a slow crack development and a less significant cumulative ringing count change are observed. When entering the stage *de*, a large number of microcracks occur in slate, and the original microcracks gradually extend and coalesce, forming macrocracks. The AE ringing count increases rapidly. The cumulative ringing counts of slate samples increase drastically, except for the slate with 0° bedding dip angle, which has a quiescent stage of 35 s. As the stress approaches to the peak stress, the AE ringing counts of samples with different bedding dip angles present a dramatic climb, and the cumulative ringing count increases exponentially. Specifically speaking, about 33.5% (0°), 32.1% (30°), 38.3% (45°), 24.3% (60°) and 54.6% (90°) ring counts are generated during less than 1% of the total time, that is, more and more cracks propagate thoroughly and eventually

form macrocracks. In stage *ef*, the stress decreases suddenly, the slate samples tend to be completely damaged, and the cumulative ringing counts increase progressively.

In conclusion, the cumulative ringing counts of 45º and 60º dip angle slates experience linear upward trends before the entire failure. The internal microcracks evolution is relatively regular and the failure process is relatively stable, which is consistent with shear slip failure characteristics. In contrast, the cumulative ringing counts of 0º, 30º and 90º slates fluctuate distinctly with severe failure process, according with the features of splitting failure. The AE ringing count unnormally increases prior to peak failure, so the sudden increase of AE ringing count can be obtained as the precursor of slate instability failure.

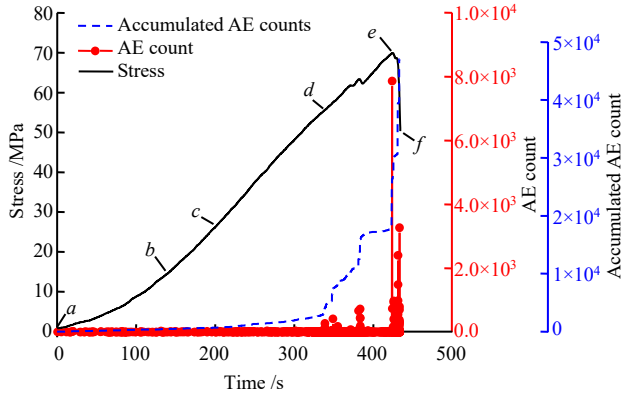

(a) $\beta=0^{\circ}$

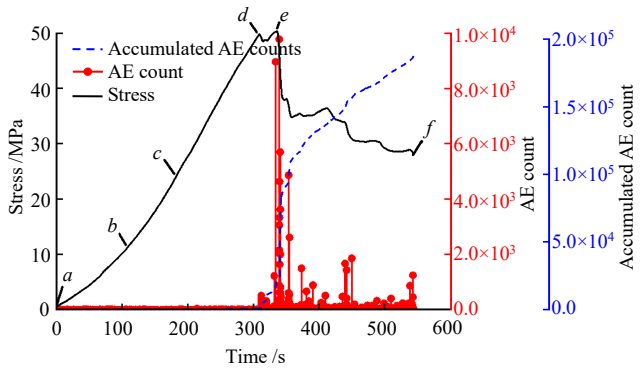

(b) $\beta=30^{\circ}$

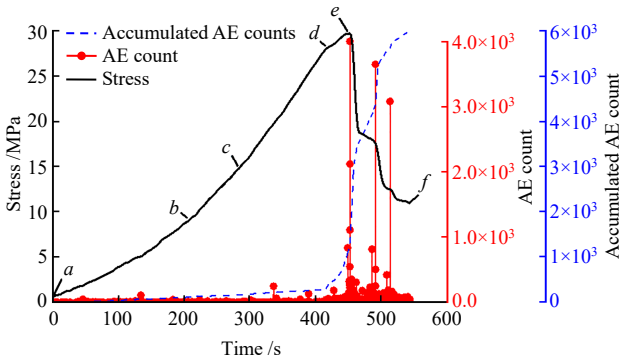

(c) $\beta=45^{\circ}$

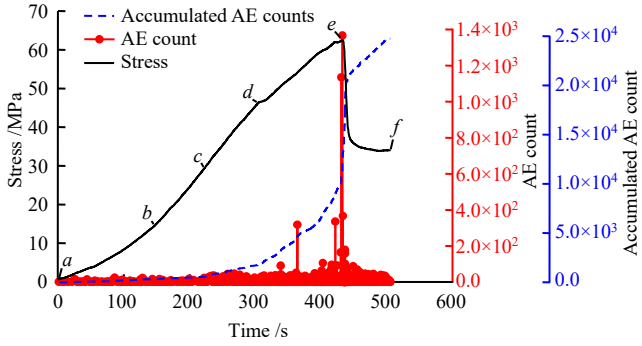

(d) $\beta=60^{\circ}$

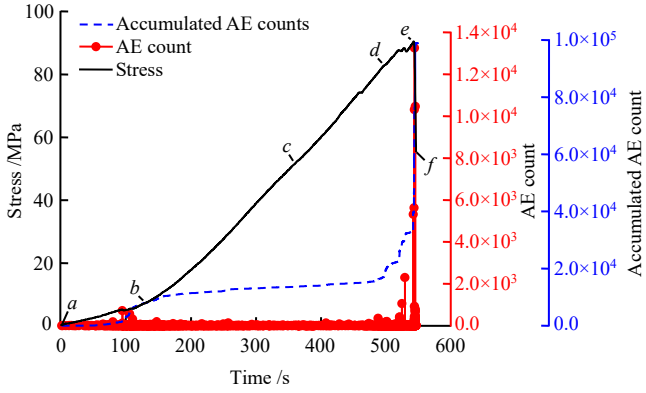

(e) $\beta=90^{\circ}$

Fig. 5 The variation curves of AE counts and cumulative AE counts for slate with different β

3.2.2 Amplitude frequency characteristics

As the main parameters of AE characteristics, amplitude and peak frequency reflect a wealth of information of slate failure. Fig.6 illustrates the relationship between amplitude, peak frequency and stress-time of slate samples in failure process. The amplitude varies from 40 dB to

60 dB, and the peak frequency varies from 50 kHz to 350 kHz, which can be divided into three categories: low frequency (50−150 kHz), medium frequency (150−250 kHz) and high frequency (250−350 kHz). Correspondingly, the amplitude range is divided into four groups: low amplitude (40−45 dB), middle amplitude (45−50 dB), high amplitude (50−55 dB) and ultra-high amplitude (55−60 dB).

As shown in Fig.6, the cracks in stages *ab* and *bc* are closed, releasing a small number of high-frequency and low-amplitude signals. With the increase of stress (*cd*), the small-scale cracks gradually propagate. A small number of low and medium frequency signals appear, the amplitude of the signals increases at the same time. In this case, the ratio of low-frequency and high-amplitude (LF-HA) signals (the ratio of the number of LF-HA signals generated by t_n (5−20 s) to the total number of signals) is about 1.7%−5.8%. In stage *de*, the original microcracks extend and coalesce into macrocracks, releasing a lot of LF signals with higher amplitudes. The ratio of LF-HA signals increases significantly, but there still remains high-frequency components, which is resulted from the macro

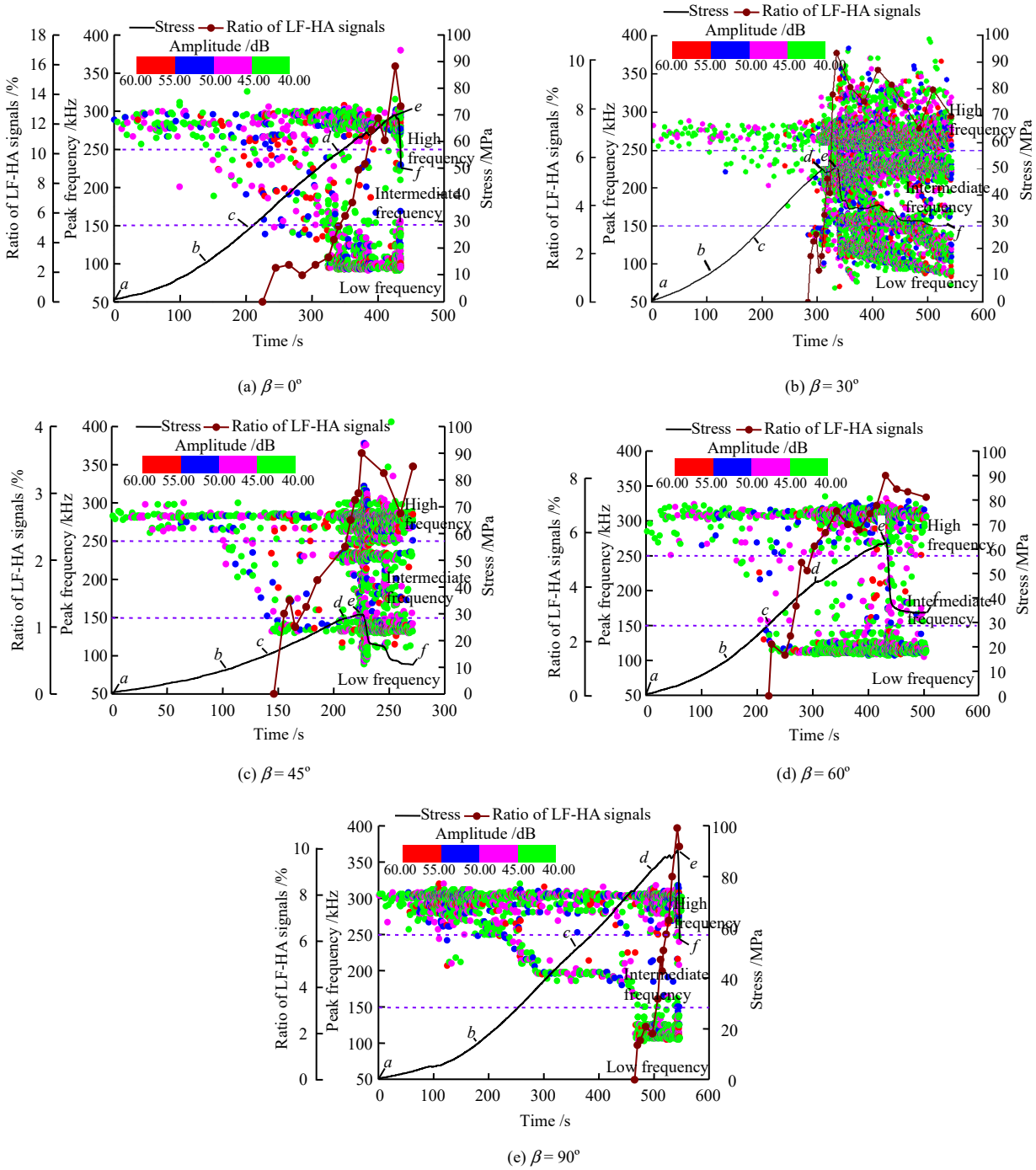

(a) $\beta = 0°$

(b) $\beta = 30°$

(c) $\beta = 45°$

(d) $\beta = 60°$

(e) $\beta = 90°$

Fig. 6 The amplitude−frequency characteristic curves of slate with different β

failure of slate containing a large number of micro-meso fractures and generating HF signals[33]. As the stress approaches to the peak, slate samples are broken, in the meanwhile, the ratio of LF-HA signals reaches its maximum, ranging from 3.6% to 15.9%. In stage *ef*, slate tends to be completely failed, and thus the ratio of LF-HA signals decreases slightly (3.4%−13.2%). Therefore, the abrupt increase in the ratio of LF-HA signals can be treated as a precursor of instability failure of layered slate[34].

Before the macro failure in slate, abundant LF-HA signals are generated, mainly concentrated in the crack transfixion stage. In general, LF-HA signals represent relatively large-scale micro failure. By comparing the ratio of LF-HA signals at crack transfixion stage, the crack propagation process before macro failure of layered slate can be further analyzed. As illustrated in Fig.7, the ratio of LF-HA signals first decreases and then increases with the increase of bedding dip angle. The number of macrocracks produced by slate with bedding dip angle of 45º is the least in crack transfixion stage.

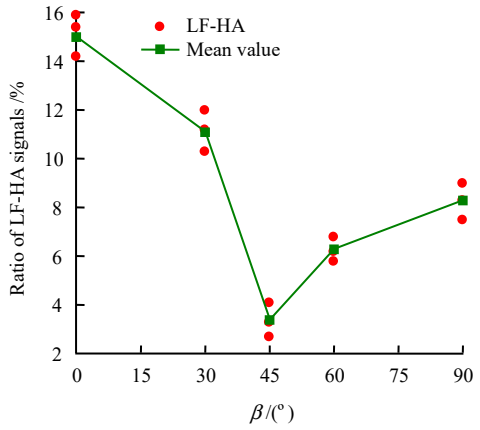

Fig. 7 Relationship curves of the proportion of low-frequency and high-amplitude signals for slate with different β

In addition, the relationship between the average frequency, AF, and the ratio of rise-time to amplitude, RA, can be used to classify the microcracks inside the rock[35], where the critical slope k (AF_{max}/RA_{max}[36]) used to distinguish shear and tensile cracks was set as 1.12. The proportion of shear cracks to total cracks is displayed in Fig.8, when the dip angle increases from 0º to 90º, the proportion of shear cracks climbs up and then declines. The proportion of shear cracks in slate with horizontal bedding and vertical bedding is lower than 20%, and the failure of slate samples is dominated by tension. However, there are more shear microcracks in 45º and 60º dip angle slates, accounting for 40%−50%, suggesting an obvious shear action. Therefore, the change of the relative number of microcracks further elucidates the transformation of failure modes of layered slate.

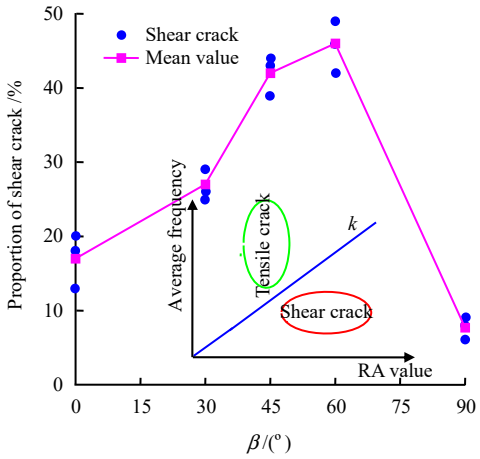

Fig. 8 Proportion of shear cracks to total cracks of layered slate

4 Multifractal characteristics

Multifractal describes the inhomogeneity and complexity of natural things in more detail. Rock failure and the resultant plenty of AE signals are nonlinear and discrete. Hence, the analysis of AE signals using multifractal method enables us to reveal the internal fracture mechanism of slate.

4.1 Multifractal spectrum

In this study, the box counting method[37] was used to calculate the multifractal spectrum of AE counting time series of layered slate. Assuming that the time series $\{T_i\}$ is divided into N subsets of length n, and the probability distribution of each subset $\{P_i(n)\}$ is calculated as[38]

$$x_q(n) \equiv \sum p_i(n)^q \sim n^{\tau(q)} \quad (1)$$

where $x_q(n)$ is the function defines allocation; $\tau(q)$ is the quality index, $-\infty<q<+\infty$, q is the weight factor, determining the non-uniformity of multifractal[25]. In general, the larger q is, the more convincing results are. However, due to the complexity of calculation, the value of Q is limited to a certain range. In this paper, Q is within −20 to 20. $\tau(q)$ is calculated by transforming Eq.(1)[39]:

$$\tau(q) = \lim_{n\to 0} \frac{\ln x_q(n)}{\ln n} \quad (2)$$

Applying Eq.(2) Legendre transform to $\tau(q)$-q, we get[40]:

$$\alpha = \frac{\mathrm{d}(\tau(q))}{\mathrm{d}q} = \frac{\mathrm{d}}{\mathrm{d}q}\left(\lim_{n\to 0}\frac{\ln x_q(n)}{\ln n}\right) \quad (3)$$

$$f(\alpha) = \alpha q - \tau(q) \quad (4)$$

where α is the singularity index, reflecting the singularity of $\{P_i(n)\}$ and the degree of non-uniformity of probability subset; $f(\alpha)$ is the fractal dimension of subset α, and represents the frequency of the AE signal subset with α singularity during the loading process. The $\alpha - f(\alpha)$ curve is the multifractal spectrum of the calculated series, showing the inhomogeneity and randomness of the signals. The larger the multifractal spectrum width $\Delta\alpha = \alpha_{\max} - \alpha_{\min}$, the more intense the signal distribution fluctuation. Subsets corresponding to $\alpha_{\max}$ and $\alpha_{\min}$ denote the low and high energy signals in time series respectively, while $f(\alpha_{\max})$ and $f(\alpha_{\min})$ mark the frequency relations of different energy signals. $f(\alpha_{\max})$ and $f(\alpha_{\min})$ are the frequencies of low and high energy signals. The smaller $\Delta f(\alpha)$ is, the more high energy signals are, and the higher the degree of rock fracture is, and vice versa[26].

4.2 Multifractal evolution of layered slate

Figure 9 shows the multifractal spectrum of AE signals of layered slate. The overall shape of multifractal spectra of slates with different bedding dip angles remain the same, and $\Delta f(\alpha)$ increases first and then decreases with the increase of $\Delta\alpha$, indicating that the fracture of layered slate is similar, while the different multifractal spectrum widths reveal different micro failure characteristics.

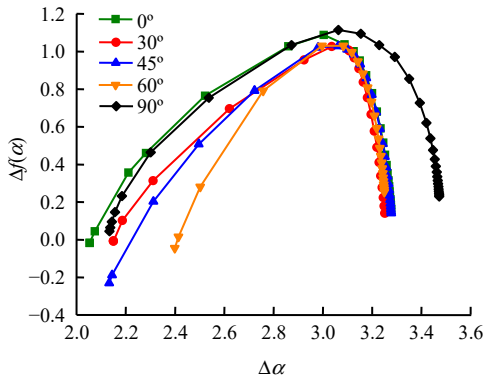

Fig. 9 Multifractal spectrum of layered slate

As shown in Fig.10, there are sizeable differences between the relationship curves of multifractal parameters $\Delta f(\alpha)$ and $\Delta\alpha$ in the loading process. In initial loading stage (ab), the internal cracks are gradually compacted, $\Delta\alpha$ is at a lower value while $\Delta f(\alpha)$ is at a higher value. $\Delta\alpha$ and $\Delta f(\alpha)$ of 0°, 30°, 45°, and 60° dip angle slates fluctuate slightly. $\Delta\alpha$ of 90° dip angle slate suddenly increases from 0.92 to 1.15 during 72−95 s, with an increase of ~25%, while $\Delta f(\alpha)$ quickly goes down from −0.43 to −0.87, with a reduction of ~102.3%, indicating numerous microcracks and obvious multifractal characteristics. In stage bc, $\Delta\alpha$ and $\Delta f(\alpha)$ of all slate samples keep stable. In stage cd, $\Delta\alpha$ suddenly rises while $\Delta f(\alpha)$ suddenly declines, and the multifractal characteristics are enhanced remarkably. When entering stage de, as the stress reaches the peak, the microcracks gradually propagate, $\Delta\alpha$ and $\Delta f(\alpha)$ of all samples rapidly fluctuate to the maximum. $\Delta\alpha$ of different layered slates all experience a sudden descent followed by an ascent. Specifically, as the dip angle increases from 0° to 90°, $\Delta\alpha$ suddenly drops to 1.28, 1.09, 1.26, 1.42 and 1.02, respectively, and then rises to 1.63, 1.26, 1.57, 1.55 and 1.30, indicating that the microcracks propagation within slate is unstable with conspicuous multifractal characteristics. Moreover, the multifractal of 0° dip angle slate has a relatively quiet period of 35 s. The lowest decrease and increase belong to 60° dip angle slate, accounting for only 0.6% and 9.2%. In the post-peak stage (ef), with the rapid reduction of stress, all samples are completely damaged, showing a sudden drop and rise of $\Delta\alpha$ and $\Delta f(\alpha)$, which tend to be stable eventually.

It is worth noting that the location of decrease and increase of $\Delta\alpha$ are discrepant for slates with different dip angles. When the bedding dip angles are 0°, 30°, 45°, 60° and 90°, the plunges of $\Delta\alpha$ correspond to 88.9%, 95.1%, 95.3%, 93.5% and 97.1% of the peak stress, while the sudden increases of $\Delta\alpha$ correspond to 99.1%, 94.0%, 98.3%, 98.6% and 97.8% of the peak stress respectively. In addition, the overall variation of multifractal spectrum width $\Delta\alpha$ corresponds to the decrease of $\Delta f(\alpha)$ during slate failure process. Therefore, the change of multifractal $\Delta\alpha$ can be selected as the instability precursor of layered slate.

5 Multifractal warning time

Figure 11 presents the damage evolution curve of layered slate, in which the damage variable D is defined as[41]

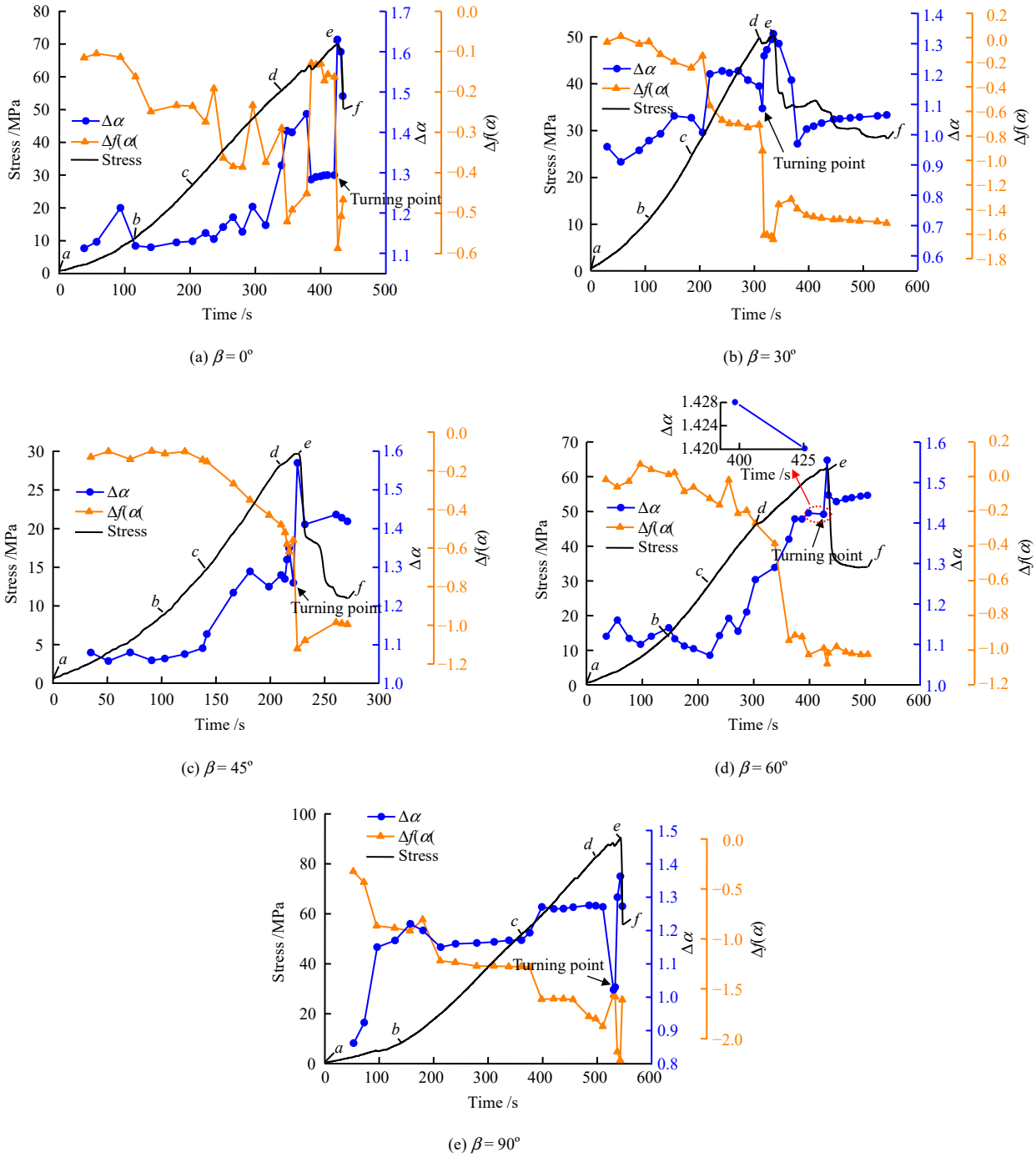

(a) $\beta=0°$ (b) $\beta=30°$

(c) $\beta=45°$ (d) $\beta=60°$

(e) $\beta=90°$

Fig. 10 Variation curves of multifractal characteristic for layered slate

$$D=\frac{\sum C_t}{C_n} \tag{5}$$

where $\sum C_t$ is the cumulative AE count from the beginning of loading to time t; C_n is the cumulative count when slate is completely broken.

As illustrated in Fig.11, in the compaction stage and elastic stage, the damage gradually intensifies, while in the initial cracking and crack transfixion stage, the damage follows a linear growth, and a large number of microcracks appear and further propagate into macrocracks. As the stress approaches the peak stress, damage variable D increases exponentially. Combined with Fig.10, it can be seen that $\Delta\alpha$ experiences a slow increase followed by a sharp increase, which is the same as the trend of damage curve. The slow increase of $\Delta\alpha$ corresponds to the gentle intension of damage, while the sudden increase of $\Delta\alpha$ attributes to the exponential growth of damage variable[27], indicating that the change of $\Delta\alpha$ can reflect the damage evolution of slate.

The sudden damage in rocks indicates the initiation of macroscopic failure. Table 1 lists the time difference

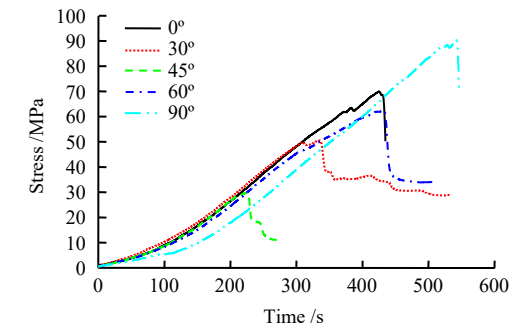

(a) Stress-time relationship

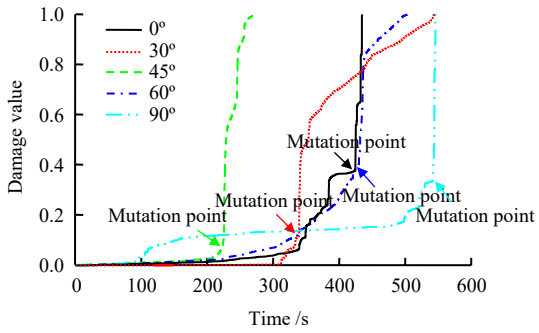

(b) Damage evolution

Fig. 11 Damage evolution curves of layered slate

Table 1 Early warning time of $\Delta\alpha$ for layered slate

Specimen number	Time of mutation /s		$\Delta\alpha$ warning time /s	
	$\Delta\alpha$	Damage variable	Value	Mean value
U0-1	403.3	408.5	5.2	
U0-2	420.8	423.9	3.1	4.8
U0-3	430.6	436.6	6.0	
U30-1	315.3	331.6	16.3	
U30-2	339.2	359.8	20.6	18.7
U30-3	321.6	340.8	19.2	
U45-1	221.3	223.3	2.0	
U45-2	210.7	214.3	3.6	2.8
U45-3	215.3	218.1	2.8	
U60-1	439.1	446.1	7.0	
U60-2	451.3	455.2	3.9	5.3
U60-3	425.6	430.7	5.1	
U90-1	511.5	520.5	9.0	
U90-2	532.0	539.9	7.9	9.4
U90-3	537.9	549.3	11.4	

between $\Delta\alpha$ surge point and damage mutation point of slate samples. From 0° to 90° dip angle, $\Delta\alpha$ is 4.8, 18.7, 2.8, 5.3 and 9.4 s earlier than the damage mutation point, respectively. The time difference between $\Delta\alpha$ mutation point and damage mutation point is defined as warning time, as shown in Fig.12, with the increase of bedding dip angle, warning time increases first, then decreases and rebounds. That is, 0°, 45° and 60° dip angle slates have short $\Delta\alpha$ warning times, while 30° and 90° dip angle samples have relatively longer $\Delta\alpha$ warning times. Among them, the longest one is 30° dip angle slate due to the small stress drop of 30° dip angle slate before damage mutation. The internal energy of slate is released momently, accompanied by the rapid propagation of cracks. $\Delta\alpha$ starts to increase suddenly at this point, accounting for a longer warning time than that of other dip angle slates.

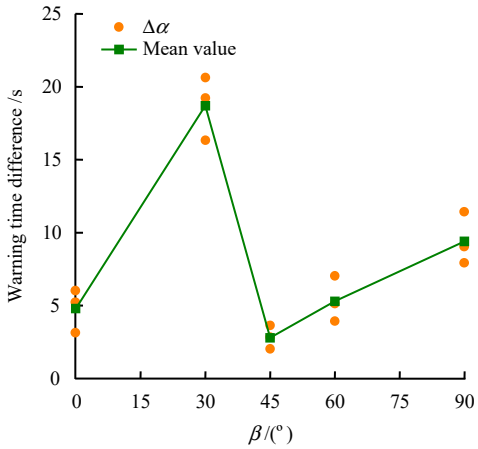

Fig. 12 Variation curve of early warning time for slate with different β

6 Conclusions

(1) Failure modes of layered slate vary greatly with the change of bedding dip angle. When the dip angle increases from 0° to 90°, the failure modes change from tension-splitting failure to splitting-shear, then to shear slip, and finally to tension-splitting.

(2) The abrupt increase in the ring count and the continuous increase in the ratio of LF-HA signals can be used as precursors to the instability of slate. The ratio of LF-HA signals decreases first and then increases with the increase of bedding dip angle in crack transfixion stage, and the order from high to low is 0°>30°>90°>60°>45°.

(3) Multifractal spectrum width $\Delta\alpha$ can also be used as a precursor to the instability of layered slate. The change of $\Delta\alpha$ reflects the damage evolution. It is found the sudden increase of $\Delta\alpha$ is earlier than the sudden increase of damage. With the increase of bedding dip angle, the $\Delta\alpha$ warning time increases first, then decreases and then rebounds. The warning time is the longest when the bedding dip angle is 30°.

References

[1] XIE Yun-peng, CHEN Qiu-nan, HE Yong-chao, et al.

Creep model construction and application of carbonaceous slate with muscovite and graphite under deep high geostress environment[J]. Journal of Central South University (Science and Technology), 2021, 52(2): 568−578.

[2] LIU Kai-de, LIU Quan-sheng, ZHU Yuan-guang, et al. Experimental study of coal considering directivity effect of bedding plane under Brazilian splitting and uniaxial compression[J]. Chinese Journal of Rock Mechanics and Engineering, 2013, 32(2): 308−316.

[3] YE Hai-wang, NING Wei-xing, LEI Tao, et al. Directivity effect of failure mode of layered slated under Brazilian spit test[J]. Journal of Wuhan University of Technology, 2016, 38(9): 91−97.

[4] TAVALLALI A, VERVOORT A. Effect of layer orientation on the failure of layered sandstone under Brazilian test conditions[J]. International Journal of Rock Mechanics & Mining Sciences, 2010, 47(2): 313−322.

[5] NING Wei-xing, YE Hai-wang, LONG Mei, et al. Splitting and failure behavior of layered slate at different angle[J]. Metal Mine, 2017(8): 58−62.

[6] OU Xue-feng, ZHANG Xue-min, ZHANG Cong et al. Study on bedding effect and damage constitutive model of slate under compressive dynamic loading[J]. Chinese Journal of Rock Mechanics and Engineering, 2019, 38(Suppl.2): 3503−3511.

[7] WU Ren-jie, LI Hai-bo, LI Xiao-feng, et al. Dynamic mechanical properties of layered phyllite subject to different impact loads[J]. Chinese Journal of Rock Mechanics and Engineering, 2019, 38(Suppl.2): 3304−3312.

[8] LI Jiang-teng, WANG Hui-wen, LIN Hang. Relationship among stratification angle, compressive strength, and fracture toughness of transversely isotropic slate[J]. Journal of Hunan University (Natural Science), 2016, 43(7): 126−131.

[9] SUN Qing-pei, ZHANG Zhi-zhen, DU Lei-ming, et al. Effect of bedding angle on mechanical and acoustic emission characteristics of layered rock[J]. Metal Mine, 2017(2): 7−13.

[10] CHU Chao-qun, WU Shun-chuan, ZHANG Shi-huai, et al. Mechanical behavior anisotropy and fracture characteristics of bedded sandstone[J]. Journal of Central South University (Science and Technology), 2020, 51(8): 2232−2246.

[11] WANG Yue-peng, LIU Xiang-jun, LIANG Li-xi. Influences of bedding planes on mechanical properties and prediction method of brittleness index in shale[J]. Lithoulogic Reservoirs, 2018, 30(4): 149−160.

[12] WANG Cong-cong, LI Jiang-teng, LIN Hang, et al. Anisotropic mechanical characteristics of slate in uniaxial compression[J]. Journal of Central South University (Science and Technology), 2016, 47(11): 3759−3764.

[13] GANNE P, VERVOORT A, WEVERS M. Quantification of pre-peak brittle damage: correlation between acoustic emission and observed micro-fracturing[J]. International Journal of Rock Mechanics and Mining Sciences, 2007, 44(11): 720−729.

[14] DIAO Xin-hong, FU Yu, HONG Peng, et al. Acoustic emission characteristics in the failure process of slate with different bedding structures[J]. Journal of Kunming University of Science and Technology (Natural Science), 2020, 45(5): 116−123.

[15] LI An-qiang, ZHANG Ru, AI Ting, et al. Acoustic emission space-time evolution rules and failure precursors of granite under uniaxial compression[J]. Chinese Journal of Geotechnical Engineering, 2016, 38(Suppl.2): 306−311.

[16] WANG Xiao-ran, WANG En-pei. LIU Xiao-fei. et al. Macro-crack propagation process and corresponding AE behaviors of fractured sandstone under different loading rates[J]. Chinese Journal of Rock Mechanics and Engineering, 2018, 37(6): 1446−1458.

[17] LI He-gui, ZHANG Ru, GAO Ming-zhong, et al. Advances in technology of acoustic emission of rock[J]. Chinese Journal of Underground Space and Engineering, 2013, 9(Suppl.1): 1794−1804.

[18] YIN Xian-gang, LI Shu-lin, TANG Hai-yan. Study on strength fractal features of acoustic emission in process of rock failure[J]. Chinese Journal of Rock Mechanics and Engineering, 2005, 24(19): 3512−3516.

[19] CONG Yu, FENG Xia-ting, ZHENG Yin-ren, et al. Experimental study on acoustic emission failure precursors of marble under different stress paths[J]. Chinese Journal of Geotechnical Engineering, 2016, 38(7): 1193−1201.

[20] XU Jie, XU Ning, JIANG Jing-dong. Research on Precursor information of sandstone failure under different loading and unloading paths based on acoustic emission monitoring[J]. Journal of Water Resources and Architectural Engineering, 2021, 19(1): 170−175, 230.

[21] YUAN R F, LI Y H. Fractal analysis on the spatial distribution of acoustic emission in the failure process of rock specimens[J]. International Journal of Minerals, Metallurgy and Materials, 2009, 16(1): 19−24.

[22] XU S L, WU W, ZHANG H, et al. Experimental study on cyclic property of rocks under uniaxial compression[C]// Proceedings of third International Conference on Experimental Mechanics. Beijing: SPIE, 2002: 261−264.

[23] KONG X G, WANG E Y, HU S B, et al. Fractal characteristics and acoustic emission of coal containing methane in triaxial compression failure[J]. Journal of Applied Geophysics, 2016, 124(11): 139−147.

[24] CAI Jiang-dong, CHEN Ya-dong, ZHANG Dao-ming. Study on the feature of acoustic emission of rock under compression experiment based on multi-fractal theory[J]. Chinese Journal of Underground Space and Engineering, 2012, 8(5): 963−968.

[25] YANG Yu-jiang, LI Yuan-hui. Multi-fractal spectra characteristics of numerical rock specimen during the fracture[J]. Chinese Journal of Computational Mechanics, 2016, 33(5): 796−801.

[26] ZHANG R, LIU J, SA Z Y. Experimental investigation on multi-fractal characteristics of acoustic emission of coal samples subjected to true triaxial loading-unloading[J]. Fractals, 2020, 28(5): 2050092.

[27] KONG X G, WANG E Y, HE X Q, et al. Time-varying multifractal of acoustic emission about coal samples subjected to uniaxial compression[J]. Chaos, Solitons and Fractals, 2017, 103(7): 571−577.

[28] XU Hong-lei. Study on acoustic emission nonlinear dynamic characteristics of prefabricated crack coal and rock samples in deformation and failure[D]. Kunming: Kunming University of Science and Technology, 2017.

[29] LI Er-qiang, ZHANG Hong-chang, ZHANG Long-fei, et al. Investigation on Brazilian tests and simulations of carbonaceous slate with different bedding angles[J]. Rock and Soil Mechanics, 2020, 41(9): 2869−2879.

[30] ZHANG X M, QU X F, GONG F Q, et al. Effects of bedding on the dynamic compressive properties of low anisotropy slate[J]. Rock Mechanics and Rock Engineering, 2018, 52(4): 981−990.

[31] LI Cun-bao, XIE He-ping, XIE Ling-zhi. Experimental and theoretical study on the shale crack initiation stress and crack damage stress[J]. Journal of China Coal Society, 2017, 42(4): 969−976.

[32] ZHAO Kui, RAN Shan-hu, ZENG Peng, et al. Effect of moisture content on characteristic stress and acoustic emission characteristics of red sandstone[J]. Rock and Soil Mechanics, 2021, 42(4): 899−908.

[33] KONG B, WANG E Y, LI Z H, et al. Acoustic emission signals frequency-amplitude characteristics of sandstone after thermal treated under uniaxial compression[J]. Journal of Applied Geophysics, 2017, 136: 190−197.

[34] LU Cai-ping, DOU Lin-ming, WU Xing-rong. et al. Experimental and empirical research on frequency -spectrum evolvement rule of rockburst precursory microseismic signals of coal-rock[J]. Chinese Journal of Rock Mechanics and Engineering, 2008, 27(3): 519−525.

[35] OHNO K, OHTSU M. Crack classification in concrete based on acoustic emission[J]. Construction and Building Materials, 2010, 24(12): 2339−2346.

[36] YUE J G, KUNNATH S K, XIAO Y. Uniaxial concrete tension damage evolution using acoustic emission monitoring[J]. Construction and Building Materials, 2020, 232: 117281.

[37] YIN Xian-long. Study on minimum box counting method based on image fractal dimension estimation[J]. Electric Application, 2006, 25(9): 93−96, 106.

[38] LI Hui-fang. The study on multifractal theory and application in image processing[D]. Xi'an: Northwestern Polytechnical University, 2004.

[39] LI Nan, LI Bao-lin, CHEN Dong, et al. Multi-fractal and time-varying response characteristics of microseismic waves during the rock burst process[J]. Journal of China University of Mining& Technology, 2017, 46(5): 1007−1013.

[40] HU Shao-bin, WANG En-yuan, LI Zhong-hui, et al. Nonlinear dynamic characteristics of electromagnetic radiation during loading coal[J]. Journal of China University of Mining & Technology, 2014, 43(3): 380−387.

[41] KONG X G, WANG E Y, HE X Q, et al. Mechanical characteristics and dynamic damage evolution mechanism of coal samples in compressive loading experiments[J]. Engineering Fracture Mechanics, 2018, 210(4): 160−169.